Electronic Supplementary Material

Volume and surface effects on two-photonic and three-photonic processes in dry co-doped upconversion nanocrystals

Bettina Grauel[1], Christian Würth[1], Christian Homann[3], Lisa Krukewitt[1,†], Elina Andresen[1], Janina Roik[2], Sebastian Recknagel[2], Markus Haase[3] (✉), and Ute Resch-Genger[1] (✉)

[1] *Federal Institute for Materials Research and Testing (BAM), Division 1.2 Biophotonics, Richard-Willstaetter-Str. 11, 12489 Berlin, Germany*
[2] *Federal Institute for Materials Research and Testing (BAM), Division 1.6 Inorganic Reference Materials, Richard-Willstaetter-Str. 11, 12489 Berlin, Germany*
[3] *Institute of Chemistry of New Materials, Department Biology/Chemistry, University Osnabrueck, Barbarastr. 7, 49076 Osnabrueck, Germany*
[†] *Present address: Department of Anesthesiology and Intensive Care Medicine, University Medical Center Rostock, Schillingallee 35, 18057 Rostock, Germany*

Supporting information to https://doi.org/10.1007/s12274-021-3727-y

Synthesis of β-$NaYF_4$ core NC doped with Er^{3+} and/or Yb^{3+} and corresponding core/shell NC

Rare-earth oleates. Rare-earth oleates were prepared according to a published procedure.[1] Briefly, 60 mmol of the rare-earth chloride were dissolved in 90 mL of water, then 54,8 g of sodium oleate, 120 mL of ethanol and 210 mL of n-hexane were added. The mixture was heated at a Schlenk-line under nitrogen atmosphere. After stirring under reflux at approximately 59 °C for 14 hours the solution was cooled to room temperature. The upper organic phase containing the oleates was separated and the solvent (hexane) removed with a rotary evaporator. The rare-earth oleate obtained as waxy solids were stored in a refrigerator.
For the synthesis of the co-doped particles, mixed rare-earth oleates were prepared. For UCNC co-doped with 20 % Yb and 2 % Er (UCNC), for instance, 46.8 mmol YCl_3, 12.0 mmol $YbCl_3$ and 1.2 mmol $ErCl_3$ were used. In an analogous way mixed rare-earth oleates were prepared for the synthesis of the particles containing only 20 % Yb (YbNC) or 2 % Er (ErNC).

Synthesis of α–$NaYF_4$ shell material. For shell growth, α–$NaYF_4$ precursor particles were used as previously described.[2] Therefore, sodium oleate and yttrium oleate in a molar ratio of 2:1 were dissolved in oleic acid and octadecene (10 mL of each solvent per mmol of yttrium oleate) by heating the mixture at 100 °C under vacuum (< 0.1 mbar) for 60 minutes. After this dissolution and degassing step, 5 mmol of solid NH_4F per one mmol of yttrium oleate were added at 100 °C under weak nitrogen flow. To remove air, the reaction vessel was subjected three times to a short vacuum (3-5 sec.) and refilled with nitrogen. Then, the mixture was heated to 200 °C with a heating rate of 10 °C/min and kept at this temperature for 1 h. After cooling to room temperature, NaF formed as by-product was removed by centrifugation. The nanoparticles were precipitated from the supernatant by adding an equal volume of ethanol and separated by centrifugation. For further purification, the precipitate was re-dispersed in hexane and precipitated with ethanol. The particles then were separated again by centrifugation and were dried at room-temperature for 24 hours before use.

Synthesis of β-$NaYF_4$ core particles for core/shell (Yb,Er doping, Yb doping, Er doping). For the synthesis of 6-7 nm β-$NaYF_4$:Yb and β-$NaYF_4$:Yb,Er core particles a molar ratio of 8:1:11 Na:RE:F was used.[2, 3] Therefore 7.5 mmol of the

Address correspondence to Markus Haase, markus.haase@uni-osnabrueck.de; Ute Resch-Genger, ute.resch@bam.de

doped rare-earth oleate and 60 mmol of sodium oleate were combined with 75 mL of oleic acid and 75 mL octadecene. The vigorously stirred mixture was degassed for 1 h at 100 °C under vacuum (<0.1 mbar). After switching to nitrogen flow, 82.5 mmol NH_4F were added to the solution without changing the temperature. To remove air, the vessel was subjected three times to a short vacuum (3-5 sec.) and refilled with nitrogen. The reaction mixture was then heated to 300 °C with a heating rate of 10 °C/min and kept at this temperature for 40 minutes when 20 % Yb single-doped oleate was used, respectively 30 minutes for 20 % Yb, 2 % Er co-doped or 2 % Er single-doped oleate were used. After cooling to room temperature, the resulting suspension was centrifuged to remove by-products such as NaF. The particles were then precipitated by adding ethanol to the supernatant. Purification of the particles was carried out as described above for the α-$NaYF_4$ particles.
To obtain larger particles, the Na:RE:F ratio was altered to values such as 5:1:8 or 1.5:1:4.5 as described previously. [3] In all cases, 7.5 mmol of the doped rare earth oleate was used.

Synthesis of core/shell particles. For the synthesis of the core/shell particles with different shell thickness, doped β-$NaYF_4$ core particles and undoped α-$NaYF_4$ particles, serving as precursor for the shell, were combined in different molar ratios ranging from 1:0.75 to 1:9 (core:shell).
Core/shell particles consisting of a 6-7 nm core particle with a 3-4 nm thick shell, for instance, were prepared by using core and shell material in a molar ratio of 1:7. Thus, 0.5 mmol of the doped 6-7 nm β-$NaYF_4$ core-material and 3.5 mmol of the α–$NaYF_4$ shell material were dissolved in 8 mL oleic acid and 8 mL octadecene. The stirred mixture was degassed for 1 hour at 100 °C and vacuum (<0.1 mbar). With a rate of 16 °C/min, the vessel was heated to 300 °C under nitrogen atmosphere and kept at this temperature for 2 hours. After cooling to room temperature, the core/shell particles were isolated und purified as described above for α-$NaYF_4$ and β-$NaYF_4$ particles.
Core/shell particles composed of a 6-7 nm core particle and a thinner shell of only 1 nm thickness were prepared by employing 6-7 nm β-$NaYF_4$ and α-$NaYF_4$ particles in a molar ratio of 1:2,4. After dissolving 1.0 mmol of the doped β-$NaYF_4$ core-material and 2.4 mmol of the α-$NaYF_4$ shell material in 6.8 mL oleic acid and 6.8 mL octadecene, the same procedure was applied as for the 1:7 ratio, except for the reaction time at 300 °C which was reduced to 50 minutes.

TEM Measurements

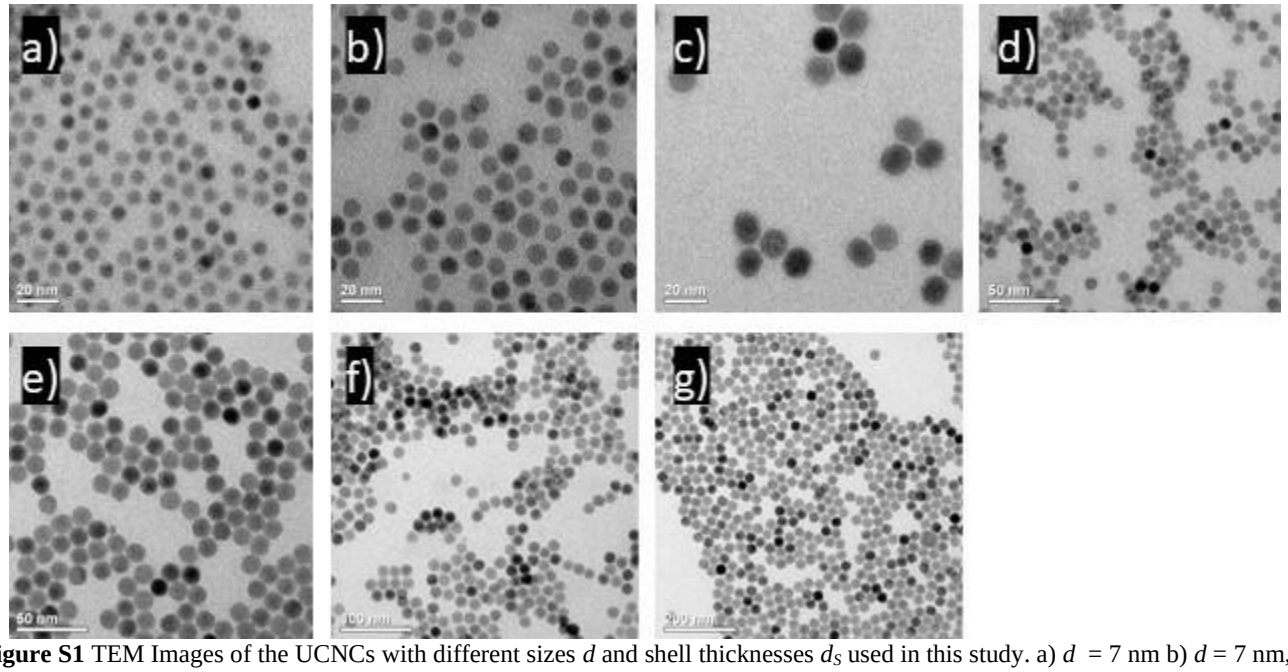

Figure S1 TEM Images of the UCNCs with different sizes d and shell thicknesses d_S used in this study. a) d = 7 nm b) d = 7 nm, d_S = 1 nm c) d = 7 nm, d_S = 3 nm d) d = 10 nm e) d = 14 nm f) d = 18 nm, and g) d = 30 nm.

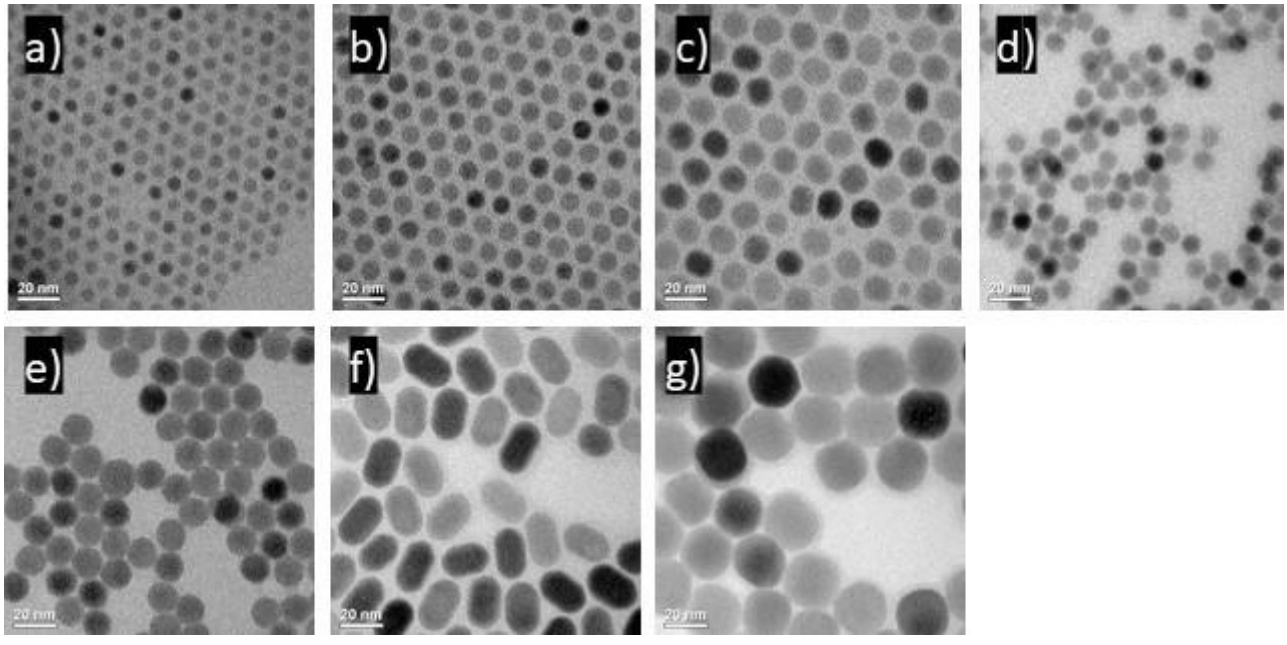

Figure S2 TEM Images of the ErNCs with different sizes d and shell thicknesses d_S used in this study. a) d = 7 nm b) d = 7 nm, d_S = 1 nm c) d = 7 nm, d_S = 3 nm d) d = 10 nm, e) d = 15 nm, f) d = 20 nm, and g) d = 28 nm.

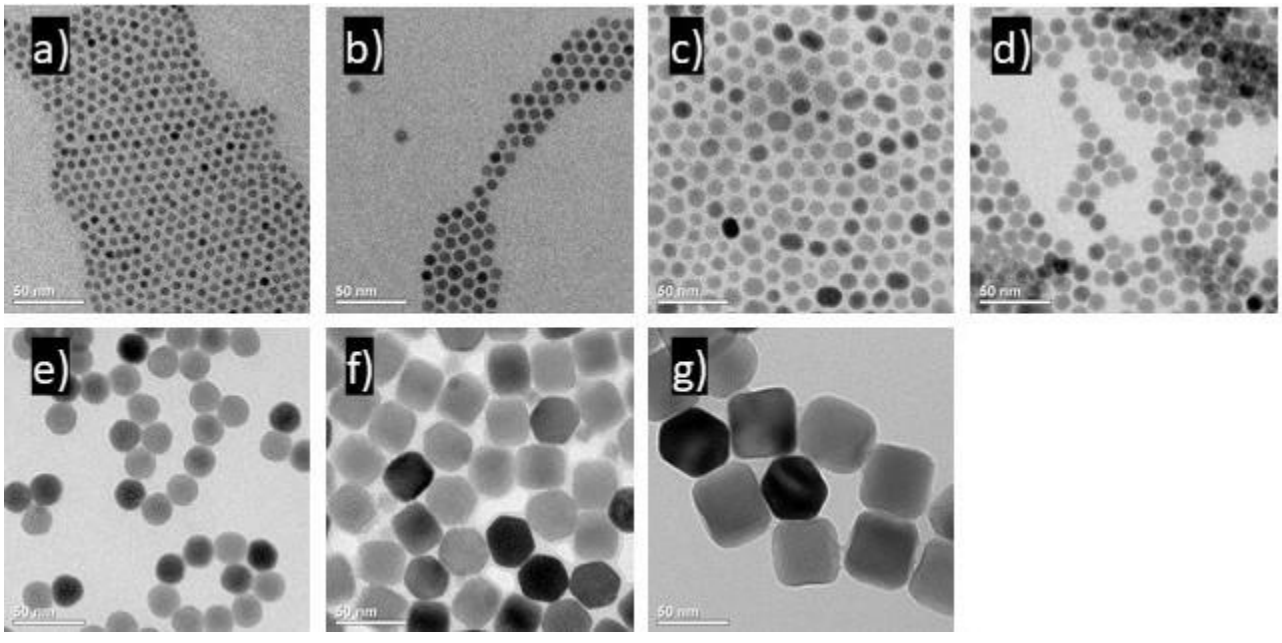

Figure S3 TEM Images of the YbNCs with different sizes d and shell thicknesses d_S used in this study. a) d = 7 nm b) d = 7 nm, d_S = 1 nm c) d = 7 nm, d_S = 3 nm, d) d = 12 nm, e) d = 22 nm, f) d = 38 nm, and g) d = 52 nm.

Table S1 Overview of the core YbNC ($NaYF_4$: 20 % Yb), ErNC ($NaYF_4$: 2 % Er), and UCNC ($NaYF_4$: 20 % Yb, 2 % Er) and the corresponding core/shell NC used in this study. Particle sizes were determined from TEM images and the thickness of the inert shell was calculated from the difference of the sizes of the core and core-shell particles. The dopant concentrations determined by ICP-OES measurements are given in the last column. For the core-shell NC, the core and core-shell NC sizes are included in the calculations (cf. Eq. S2-S3), propagating the uncertainties from our TEM measurements.

Expected doping conc.	Size [nm]	Core size [nm]	Thickness of $NaYF_4$ shell [nm]	Core dopant concentrations derived from ICP-OES measurements (mol%)		
				Er^{3+}	Yb^{3+}	Y^{3+}
20 % Yb	6.6 ± 0.4	---	---	0 ± 0	19.4 ± 0.4	80.6 ± 1.6
20 % Yb	8.3 ± 0.9	6.7 ± 0.7	0.8 ± 0.6	0 ± 0	18 ± 8	82 ± 8
20 % Yb	11.8 ± 2.5	6.6 ± 0.4	2.6 ± 1.3	0 ± 0	30 ± 20	70 ± 20
20 % Yb	12.0 ± 0.6	---	---	0 ± 0	18.7 ± 0.4	81.3 ± 1.9
20 % Yb	22.0 ± 2.0	---	---	0 ± 0	19.3 ± 0.3	80.7 ± 1.8
20 % Yb	38.0 ± 2.0	---	---	0.14 ± 0.01	19.2 ± 0.2	80.7 ± 1.8
20 % Yb	51.9 ± 2.3	---	---	0 ± 0	17.6 ± 0.1	82.4 ± 1.8
2 % Er	7.3 ± 0.6	---	---	1.92 ± 0.01	0.25 ± 0.02	97.8 ± 2.1
2 % Er	8.4 ± 0.7	6.6 ± 0.8	0.9 ± 0.5	1.1 ± 0.5	0.3 ± 0.2	98.5 ± 0.5
2 % Er	13.4 ± 0.8	7.3 ± 0.6	3.1 ± 0.5	1.1 ± 0.3	0.8 ± 0.3	98.1 ± 0.4
2 % Er	9.9 ± 0.7	---	---	1.95 ± 0.01	0 ± 0	98.1 ± 2.2
2 % Er	15.0 ± 1.0	---	---	1.95 ± 0.01	0 ± 0	98.1 ± 1.8
2 % Er	20.0 ± 1.0	---	---	1.84 ± 0.00	0.01 ± 0.00	98.2 ± 2.8
2 % Er	28.0 ± 2.0	---	---	1.93 ± 0.01	0.05 ± 0.01	98.0 ± 2.2
2 % Er, 20 % Yb	7.1 ± 0.9	---	---	2.00 ± 0.01	18.9 ± 0.4	79.1 ± 1.6
2 % Er, 20 % Yb	8.3 ± 1.0	7.1 ± 0.9	0.6 ± 0.7	1.6 ± 0.8	14 ± 7	84 ± 7
2 % Er, 20 % Yb	14.0 ± 2.4	7.1 ± 0.9	3.5 ± 1.3	2.1 ± 1.3	20 ± 13	78 ± 13
2 % Er, 20 % Yb	9.5 ± .6	---	---	2.03 ± 0.01	77.6 ± 0.3	20.4 ± 1.9
2 % Er, 20 % Yb	13.6 ± 0.9	---	---	2.04 ± 0.01	77.9 ± 0.4	20.1 ± 1.8
2 % Er, 20 % Yb	18.0 ± 1.0	---	---	1.94 ± 0.02	78.7 ± 0.3	19.4 ± 1.8
2 % Er, 20 % Yb	30.0 ± 2.0	---	---	1.95 ± 0.01	78.9 ± 0.3	19.2 ± 1.8

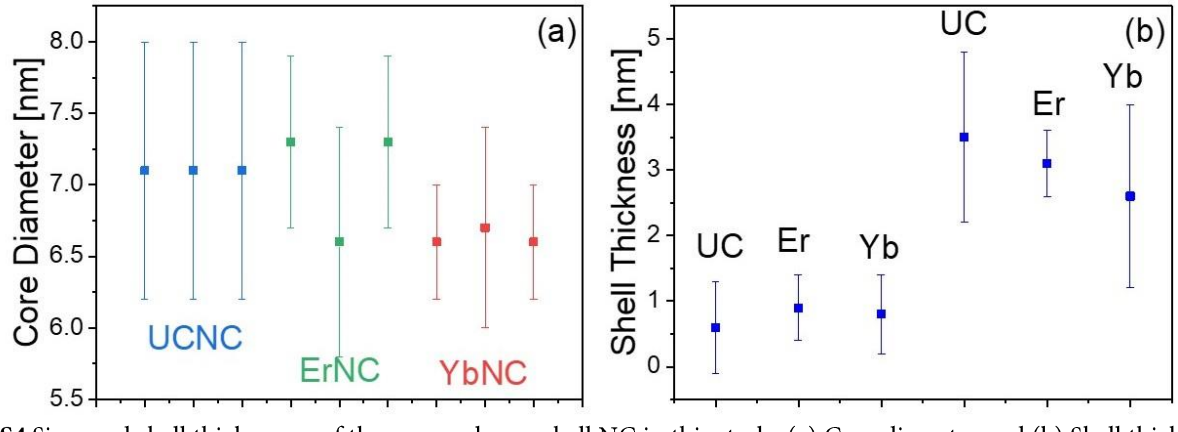

Figure S4 Sizes and shell thicknesses of the core and core-shell NC in this study. (a) Core diameter and (b) Shell thicknesses of the YbNC, ErNC, and UCNC samples studied. The diameters were obtained from TEM measurements and the shell thicknesses were derived from the differences of the diameters of the core and the core-shell particles.

We determined the molar concentrations of Er^{3+}, Yb^{3+}, and Y^{3+} in the core-shell particles from ICP-OES

measurements performed by Janina Roik and Elina Andresen.
From the amounts of Er^{3+}, Yb^{3+}, and Y^{3+} ions in the entire particle, N_{Er}, N_{Yb} und N_Y, and the volume of the entire particle, V_{tot}, as well as the volume of the core particles, V_{core}, which are both determined by TEM measurements, the amount of lanthanide ions in the core is calculated according to eq. (S1).

$$N_{Ln,core} = (N_{Er} + N_{Yb} + N_Y) \cdot \frac{V_{core}}{V_{tot}} \qquad \text{eq. (S1)}$$

The amount of Er^{3+} in the core (given in mol%) is determined as follows:

$$\%Er = \frac{N_{Er}}{N_{Ln,core}} = \frac{N_{Er}}{N_{Er} + N_{Yb} + N_Y} \cdot \frac{V_{tot}}{V_{core}} \qquad \text{eq. (S2)}$$

The amount of Yb^{3+} in the core (given in mol%) is determined analogously:

$$\%Yb = \frac{N_{Yb}}{N_{Ln,core}} = \frac{N_{Yb}}{N_{Er} + N_{Yb} + N_Y} \cdot \frac{V_{tot}}{V_{core}} \qquad \text{eq. (S3)}$$

The results given in Table (S1) include uncertainties computed using Gaussian error propagation. Since this calculation includes the size measurements, the measurement uncertainties of which exceed those of the ICP-OES measurements, the final results reveal relatively large uncertainties. As these results are merely complementary measurements to the straightforward ICP-OES results obtained for the core-only particles, they can be regarded as a confirmation of the expected dopant concentrations, as the desired Er^{3+} and/or Yb^{3+} doping concentrations of 2% and 20% mostly match with these concentrations when considering the experimentally obtained measurement uncertainties.

Determination of the total ion numbers
For every sample, the size was determined from TEM images (see Fig. S1-S3) and the statistical uncertainty is resulting from an average over several (hundreds of) particles. Using Eq.'s. (S4)[4] and (S5), the number of ions in the active core was determined, assuming doping concentrations of 20 % Yb^{3+} and 2 % Er^{3+} (not measured).

$$V_{unit\ cell} = 2 \cdot \frac{\sqrt{3}}{4} \cdot a^2 \cdot c \qquad \text{eq. (S4)}$$

$$N_{ions} = 1.5 \cdot V_{unit\ cell} \cdot c_{Ions} \cdot N_{unit\ cells} \qquad \text{eq. (S5)}$$

In Eq. (S4), the volume of one unit cell, $V_{unit\ cell}$, is determined using the lattice parameters *a* and *c* for the hexagonal lattice structure of β-$NaYF_4$ (a = 5.96 Å, c = 3.53 Å)[4]. In Eq. (S5), the number of active ions in the core, N_{ions}, is determined, where c_{Ions} is the doping concentration of active ions in the core (2 % for Er^{3+}, 20 % for Yb^{3+}) and $N_{unit\ cells}$ denotes the number of unit cells in the core, which is obtained by dividing the volume of the core (assuming a spherical particle) by $V_{unit\ cell}$. The uncertainties stem from the size distributions of the particles in the TEM images.

Table S2 Overview of selected co-doped (UCNC) and single-doped (ErNC, YbNC) particles used in this study. The diameter of the sample (d) is given as well as the total number of Er^{3+} (N_{Er3+}) and Yb^{3+} ions (N_{Yb3+}), determined using equations eq. (S4) and eq. (S5). To illustrate how drastic the numbers of sensitizer and activator ions differ for particles of different sizes, we display mean Yb^{3+} and Er^{3+} ion numbers for particles of different sizes. The uncertainties are propagated from the standard deviations of the size determination from TEM images.

Doping	d (nm)	N_{Er3+}	N_{Yb3+}
20 % Yb, 2 % Er	7.1 ± 0.9	52 ± 20	520 ± 200
20 % Yb, 2 % Er	18 ± 1	840 ± 140	8400 ± 1400
20 % Yb, 2 % Er	30 ± 2	3900 ± 800	39000 ± 8000
2 % Er	7.3 ± 0.6	56 ± 14	-
2 % Er	19.7 ± 0.8	1110 ± 130	-
2 % Er	28 ± 2	3200 ± 700	-
20 % Yb	6.6 ± 0.4	-	420 ± 80
20 % Yb	51.9 ± 2.3	-	202000 ± 27000

Optical characterization of NC and bulk materials

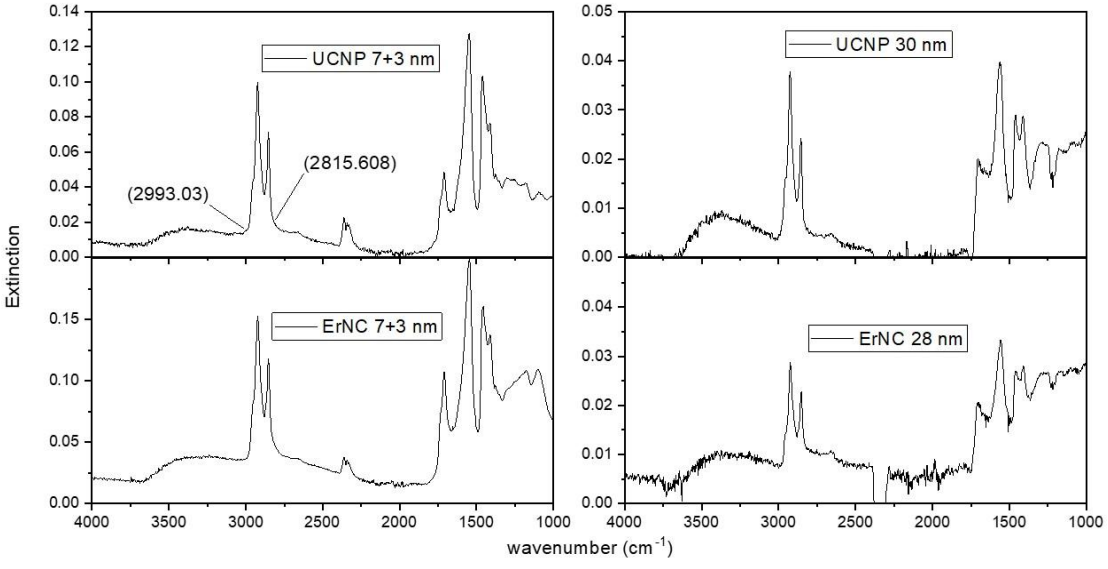

Figure S5 ATR FTIR measurements of ErNC and UCNC core and core-shell particles.

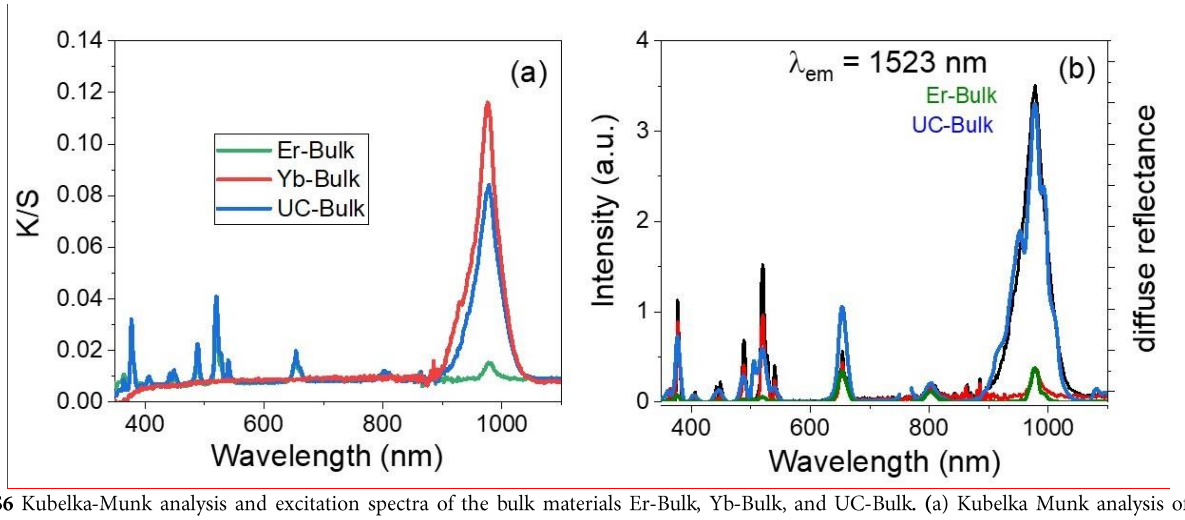

Figure S6 Kubelka-Munk analysis and excitation spectra of the bulk materials Er-Bulk, Yb-Bulk, and UC-Bulk. (a) Kubelka Munk analysis of diffuse reflectance measurements of Er-, Yb- and UC-bulk materials. b) Spectrally corrected luminescence excitation spectra of the bulk phosphors UC-Bulk (blue) and Er-Bulk (green), and Kubelka-Munk analysis of the diffuse reflectance spectrum of Er-Bulk (red) and YbEr-Bulk (black). The excitation spectra of Er-Bulk and UC-Bulk were recorded at 1523 nm. Second-order peaks were manually removed from the luminescence excitation spectra.

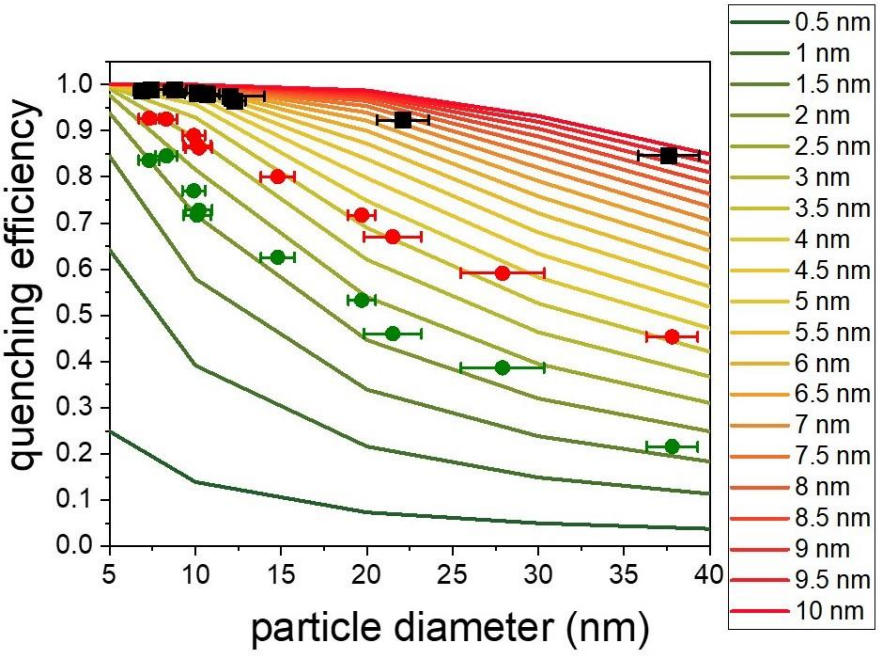

Figure S7 Quenching efficiency of the red, green, and Yb^{3+} emission (measured, dots) and theoretical volume-weighted quenching efficiencies for different Förster radii (lines).

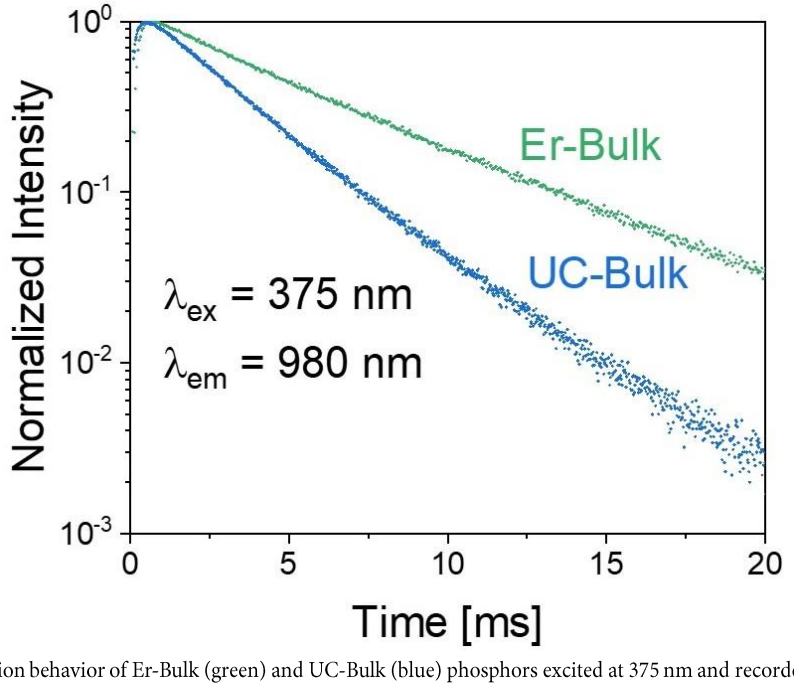

Figure S8 Time-resolved emission behavior of Er-Bulk (green) and UC-Bulk (blue) phosphors excited at 375 nm and recorded at 980 nm.

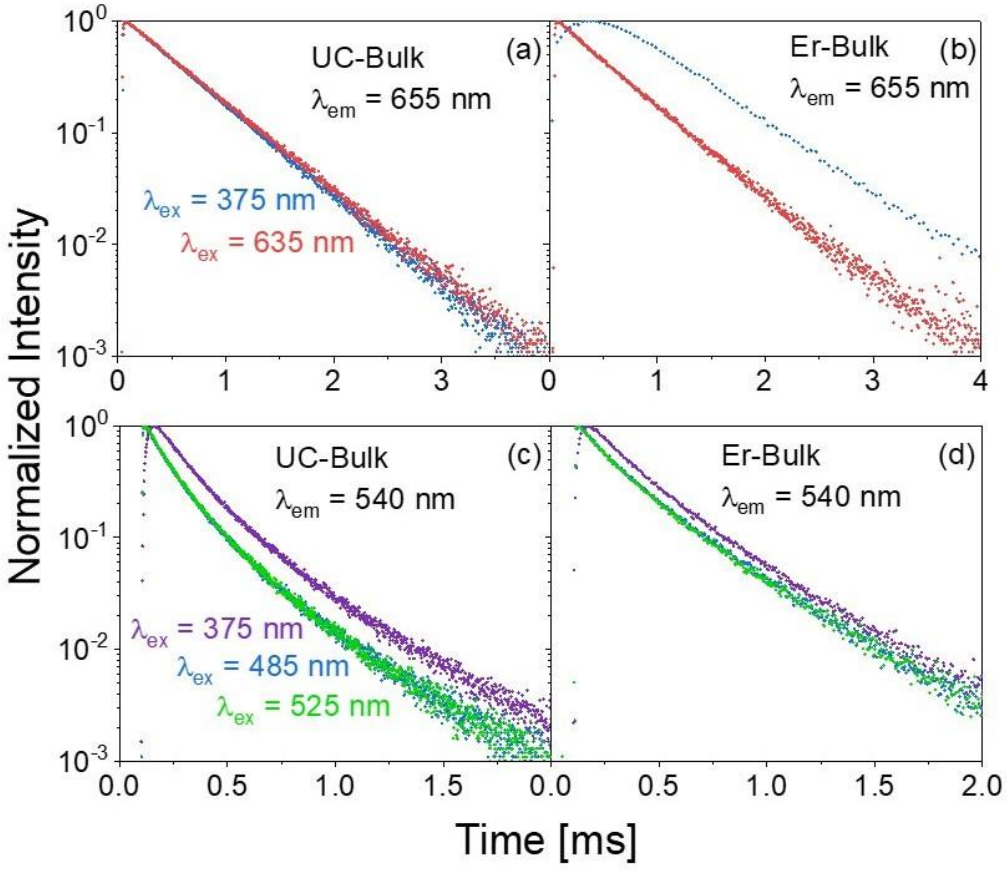

Figure S9 Time-resolved emission behavior of solid bulk phosphors: Red emission at 655 nm of a) UC-Bulk and b) Er-Bulk, excited at 375 nm (blue) and 635 nm (red), and green emission at 540 nm of c) UC-Bulk and d) Er-Bulk, excited at 375 nm (purple), 485 nm (blue), and 525 nm (green), respectively.

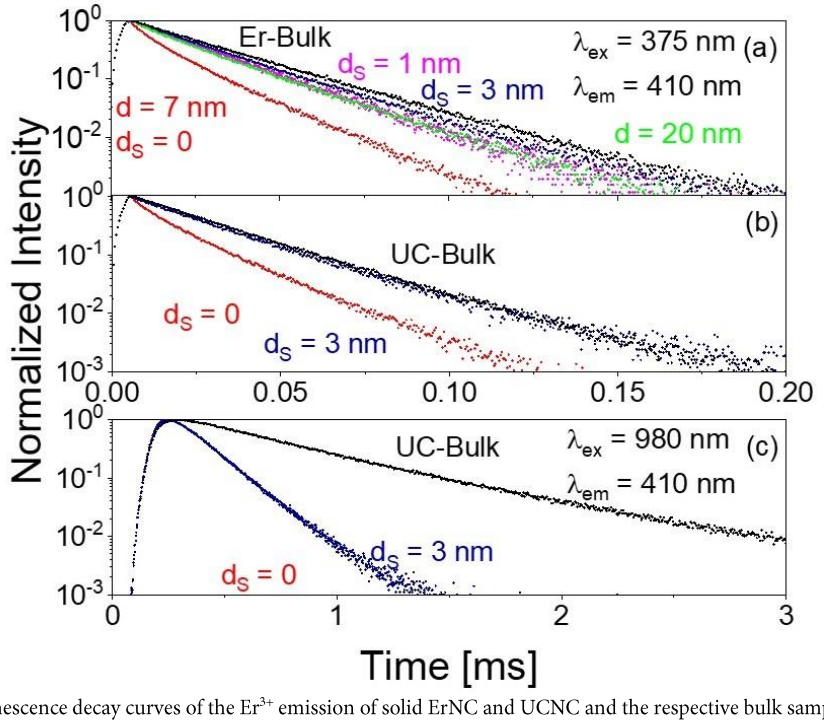

Figure S10. Normalized luminescence decay curves of the Er^{3+} emission of solid ErNC and UCNC and the respective bulk samples Er-Bulk and UC-Bulk, recorded at 410 nm. a) Core-only ErNC with mean particle diameters of 7 nm (red) and 20 nm (green), core-shell ErNC with a 7 nm core and a 1 nm shell (purple) and a 3 nm shell (navy), and Er-Bulk (black), excited at 375 nm. Core-only 7 nm UCNC unshelled (red) and with 3 nm shell (navy) and UC-Bulk (black) b) under 375 nm excitation and c) under 978 nm excitation.

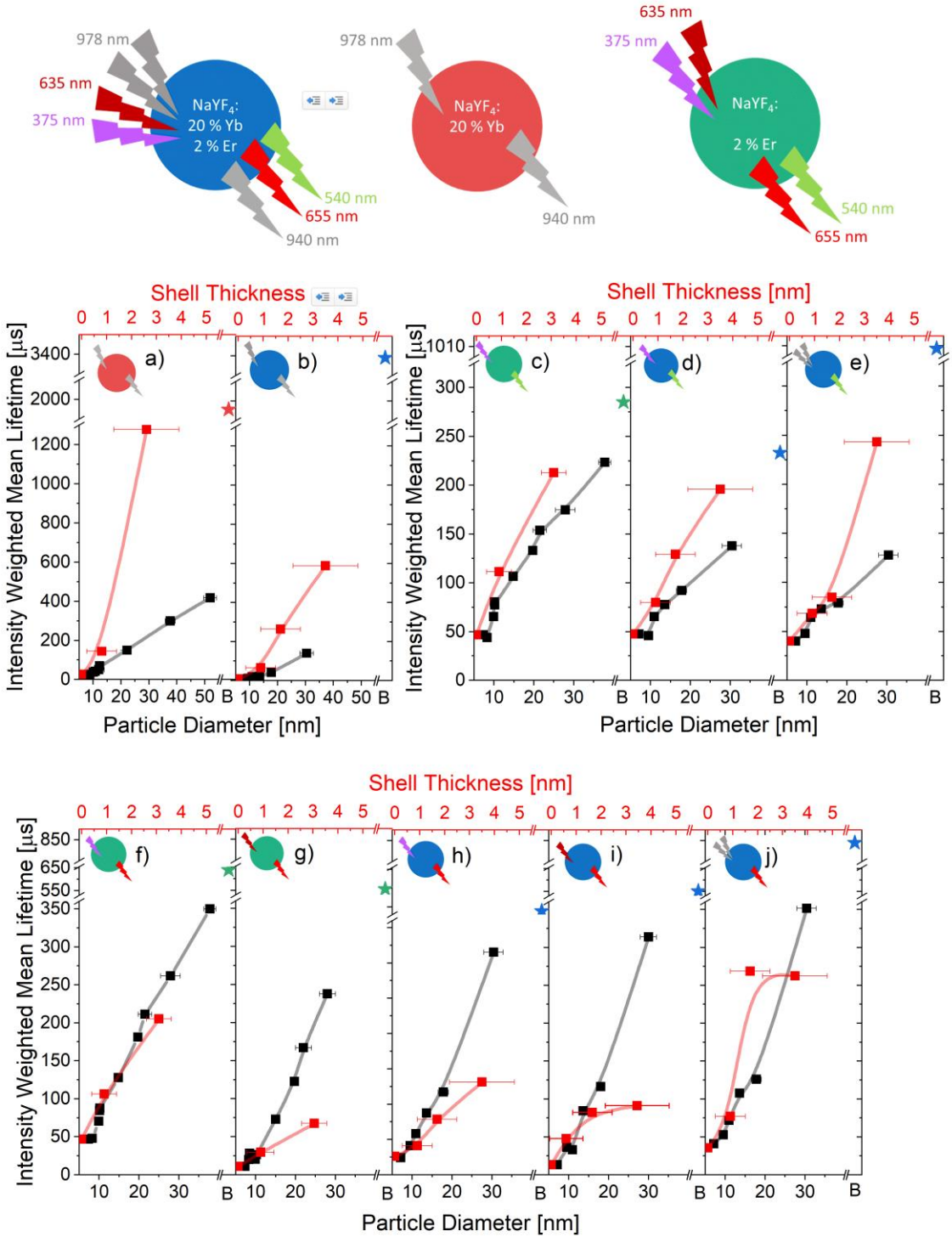

Figure S11 Intensity-weighted mean lifetimes (τ_{int}) of core (black squares) and core-shell (red squares) $NaYF_4$:Er (green icon), $NaYF_4$:Yb (red icon), and $NaYF_4$:Yb,Er (blue icon) nanocrystals, obtained from multiexponential fitsg of the 940 nm (a, b), 540 nm (c, d, e) and 655 nm (f, g, h, i, j) emission of nanocrystalline powder samples and the respective bulk materials under laser excitation at λ_{ex} = 375 nm (c, d, f, h), λ_{ex} = 635 nm (g, i), and λ_{ex} = 978 nm (a, b, e, j). The colors of the lightenings in the icons illustrate the excitation and emission wavelengths as indicated above the panels. The values of the bulk materials include as stars and are denoted as "B" on the size and shell thickness scales. The lines are only a guide for the eye.

Table S3 Intensity-weighted mean lifetimes of Er^{3+}-single-doped, Yb^{3+}-single-doped, and Yb^{3+},Er^{3+}-co-doped particle systems under 375 nm, 635 nm, and

978 nm excitation.

Doping	Core Size [nm]	Shell Thickness [nm]	Intensity-weighted mean lifetime τ_{int} [μs]					
			λ_{em} = 540 nm		λ_{em} = 655 nm			λ_{em} = 940 nm
			λ_{ex} = 375 nm	λ_{ex} = 978 nm	λ_{ex} = 375 nm	λ_{ex} = 635 nm	λ_{ex} = 978 nm	λ_{ex} = 978 nm
Yb	6.6 ± 0.4	---	---	---	---	---	---	26.6
Yb	6.7 ± 0.7	0.8 ± 0.6	---	---	---	---	---	144
Yb	6.6 ± 0.4	2.6 ± 1.3	---	---	---	---	---	1277
Yb	12.0 ± 0.6	---	---	---	---	---	---	70.0
Yb	22 ± 2	---	---	---	---	---	---	150
Yb	38 ± 2	---	---	---	---	---	---	300
Yb	52 ± 2	---	---	---	---	---	---	418
Yb (Bulk)	---	---	---	---	---	---	---	1950
Er	7.3 ± 0.6	---	46.8	---	47.0	11.3	---	---
Er	6.6 ± 0.8	0.9 ± 0.5	111	---	106	29.8	---	---
Er	7.3 ± 0.6	3.1 ± 0.5	213	---	205	67.6	---	---
Er	9.9 ± 0.7	---	65.6	---	70.7	20.5	---	---
Er	15 ± 1	---	107	---	128	73.0	---	---
Er	20 ± 1	---	133	---	181	123	---	---
Er	28 ± 2	---	175	---	262	238	---	---
Er	38 ± 2	---	223	---	350	---	---	---
Er (Bulk)	---	---	285	---	641	556	---	---
Er,Yb	7.1 ± 0.9	---	47.6	40.3	24.3	13.3	40.8	8.5
Er,Yb	7.1 ± 0.9	0.6 ± 0.7	80.1	68.5	38.3	47.9	88.2	64.8
Er,Yb	7.1 ± 0.9	1.7 ± 0.8	129	85.0	73.3	82.2	307	265
Er,Yb	7.1 ± 0.9	3.5 ± 1.3	196	243	122	91.2	301	588
Er,Yb	9.5 ± 0.6	---	45.9	48.0	41.4	36.3	52.7	11.0
Er,Yb	13.6 ± 0.9	---	77.8	73.0	87.3	84.3	108	22.0
Er,Yb	18 ± 1	---	92.2	79.1	117	116	126	42.0
Er,Yb	30 ± 2	---	138	128	315	314	351	140
Er,Yb (Bulk)	---	---	233	1007	539	550	849	3390

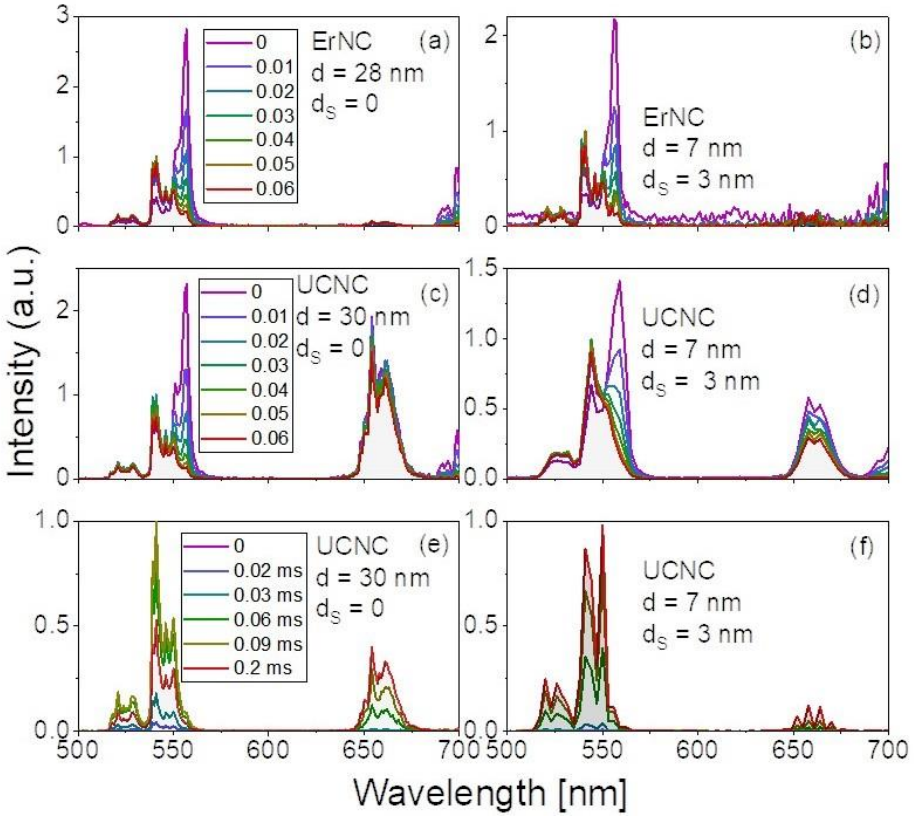

Figure S12: Time-resolved emission spectra of core and core-shell UCNC and ErNC obtained with pulsed excitation. (a) 28 nm unshelled ErNC and (b) 7 nm ErNC with 7 nm shell, excited at 375 nm. (c) 30 nm unshelled UCNC and (d) 7 nm UCNC with 7 nm shell, excited at 375 nm. The spectra are shown for time intervals after the excitation pulse, indicated in the legend. (e) 30 nm unshelled UCNC and (f) 7 nm UCNC with 7 nm shell, excited at 978 nm. Due to the slow ETU excitation, the time intervals chosen are bigger than for 375 nm excitation. The spectra for the latest time interval are filled in grey.

Description of the Monte Carlo simulation / Random Walk model

We set up a Monte Carlo model of the upconversion process in a $NaYF_4$:20 % Yb^{3+}, 2 % Er^{3+} particle of radius *R* based on a three-dimensional random walk of the excited states in the Ln^{3+} ion host lattice. The model is derived from the work of Zuo et al.[5], who examined the dynamics of two-state Yb^{3+} ions (two states) and Er^{3+} ions (three states). Upconversion occurs when two or more excited states "collide" into one Er^{3+} ion. We further developed this model by adding another excited state to the Er^{3+} ion (state 6 in Fig. S3), to allow for two- and three-photonic UC processes and obtain a better representation of the multi-photonic nature of UC.

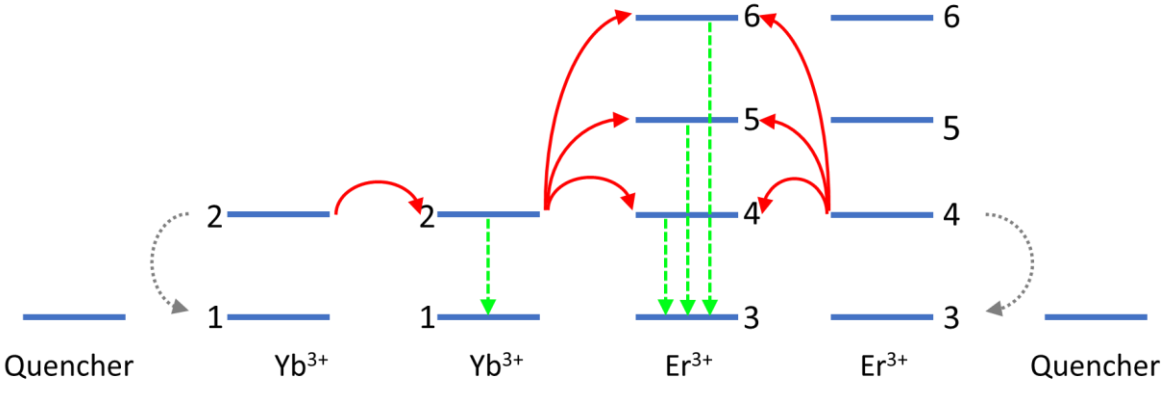

Figure S13 Schematic energy diagram with all possible interactions. Solid red arrows indicate energy transfer, dashed green arrows indicate radiative deactivation, and dotted gray arrows indicate quenching.

In accordance with the work from Zuo et al.[5], the model includes light absorption, energy migration between

Er^{3+} and Yb^{3+} ions (Yb^{3+} -> Er^{3+}, Er^{3+}->Yb^{3+}), and radiative relaxation from excited states to the ground state. We omitted, however, the ability of this model to account for the UC behavior of multi-layer systems since our studies focus on uniformly doped particles. The simulation relies on a simple cubic host lattice, even though this does not represent the experimentally realized hexagonal structure of beta-$NaYF_4$, because this crystal phase can be easier simulated, rendering it less error-prone.

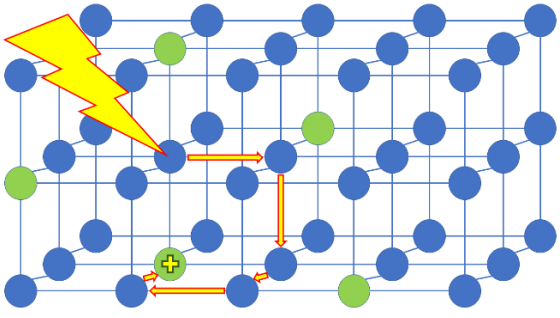

Figure S14 Schematic representation of Yb^{3+} ions (blue) and Er ions^{3+} (green) in a cubic lattice, with absorption (lightening), energy migration (arrows) and excited state of an Er^{3+} ion (plus sign).

The absorption and energy transfer rates reported by Zuo et al.[5] are included in our model. The emissive rates were obtained experimentally by us and are very similar to the rates from Zuo et al.[5]. Since our model has been further developed by the consideration of an additional Er^{3+} energy level, two energy transfer rates could not be taken from previous results and had to be determined by us (2->6, 4->6). The parameters adopted from Zuo et al.[5] in Table S4 are highlighted by an asterisk. The parameters used by Zuo et al. and by us were obtained from particles with a hexagonal host lattice and are therefore specific for β-$NaYF_4$, as they contain all relevant non-radiative information of the host.

Table S4: Simulation parameters used for the Monte Carlo simulation in this work; values taken from Zuo et al. are highlighted by an asterisk (*). The recombination rates are determined from the measured lifetimes τ_{int} and given for (7 nm core unshelled / 7 nm core + 3 nm shell" / 30 nm core unshelled). They were obtained from luminescence decay measurements after direct excitation of the respective states. For (6), the red emission was used. For (4), the 940 nm emission of ErNCs of the same size and shell thickness was employed, since the Er^{3+} emission in UCNCs at 980 nm cannot be separated from the dominant Yb^{3+} emission.

Parameters	**Value**
Total simulation time*	3 s
Time step	$2 \cdot 10^{-6}$ µs
Absorption cross section of (1)*	$1.17 \cdot 10^{-20}$ cm^{-2}
Absorption cross section of (3)*	$1.7 \cdot 10^{-21}$ cm^{-2}
Energy migration rate of (2) -> (2)*	10^5 s^{-1}
Energy migration rate of (2) -> (4)*	$2.5 \cdot 10^4$ s^{-1}
Energy migration rate of (2) -> (5)*	$3.2 \cdot 10^3$ s^{-1}
Energy migration rate of (2) -> (6)	$3 \cdot 10^4$ s^{-1}
Energy migration rate of (4) -> (2)*	10^4 s^{-1}
Energy migration rate of (4) -> (4)*	$5 \cdot 10^3$ s^{-1}
Energy migration rate of (4) -> (5)*	600 s^{-1}
Energy migration rate of (4) -> (6)	100 s^{-1}
Surface quenching rate*	10^5 s^{-1}
Recombination rate of (2) (= t_{meas}^{-1})	$(7 \cdot 10^4 / 1.2 \cdot 10^3 / 5 \cdot 10^3)$ s^{-1}
Recombination rate of (4) (=t_{meas}^{-1})	$(3.2 \cdot 10^3 / 8.4 \cdot 10^2 / 2.1 \cdot 10^3)$ s^{-1}
Recombination rate of (5) (=t_{meas}^{-1})	$(2 \cdot 10^4 / 5 \cdot 10^3 / 6.5 \cdot 10^3)$ s^{-1}
Recombination rate of (6) (=t_{meas}^{-1})	$(5 \cdot 10^4 / 1.2 \cdot 10^4 / 3.5 \cdot 10^3)$ s^{-1}
Quantum yield of states (4) and (5)*	0.5

Construction of the Simulation Model

Construction of the lattice: The particle radius *R* is an additional parameter in the script. Since the real particles are hexagonal, the total ion number inside the real particles differs from the total ion number in a cubic particle of identical size. To consider this difference, the ion number in the real particle is determined using equations Eq. (S4) and Eq. (S5) and a spherical particle with a cubic host lattice containing this ion number is constructed. The model only takes Yb^{3+} and Er^{3+} ions into account and assumes

equal spacing between nearest neighbors within the particle. The ions inside the particle are Yb^{3+} and Er^{3+} ions randomly distributed with a ratio of 10 to 1, according to the doping concentration of 20 % Yb^{3+} ions and 2 % Er^{3+} ions used.

Zuo et al.[5] gave a very detailed explanation of the determination of the simulation parameters. As we utilized all relevant parameters from this publication, no additional explanations are provided. The surface quenching rate is adopted from Zuo et al.[5] as well, but since our particles are constructed spherically, the influence of the surface on the UC processes in the particle should be different, as interactions only occur between nearest neighbors. In order to tune surface quenching, the surface quenching rate is multiplied by a factor *Q*, ranging from 0 to 1. Here, a value of zero corresponds to perfect surface passivation and shielding (no surface quenching), which mimicks a perfect inert (sufficiently thick) surface shell.

Steps in the model

At the beginning of every simulation, the host lattice of the particle is constructed, the active lanthanide ions are randomly distributed, here with ratio of 10/1 for Yb/Er, and every ion is in the electronic ground state. For each time step of 2 μs, every ion can absorb a photon with a certain probability, which depends on the ion type and the incident excitation power density, and the Ln^{3+} ions in excited states can undergo energy transfer or radiative relaxation. After every ion has been successively scanned, the next time step repeats this iteration, until the sum of the time steps equals the total measurement time of 3 s, which corresponds to 1.5 million iterations over the entire particle. For further explanations of the pump absorption and energy transfer processes in the simulation we refer to the work by Zuo et al[5]..

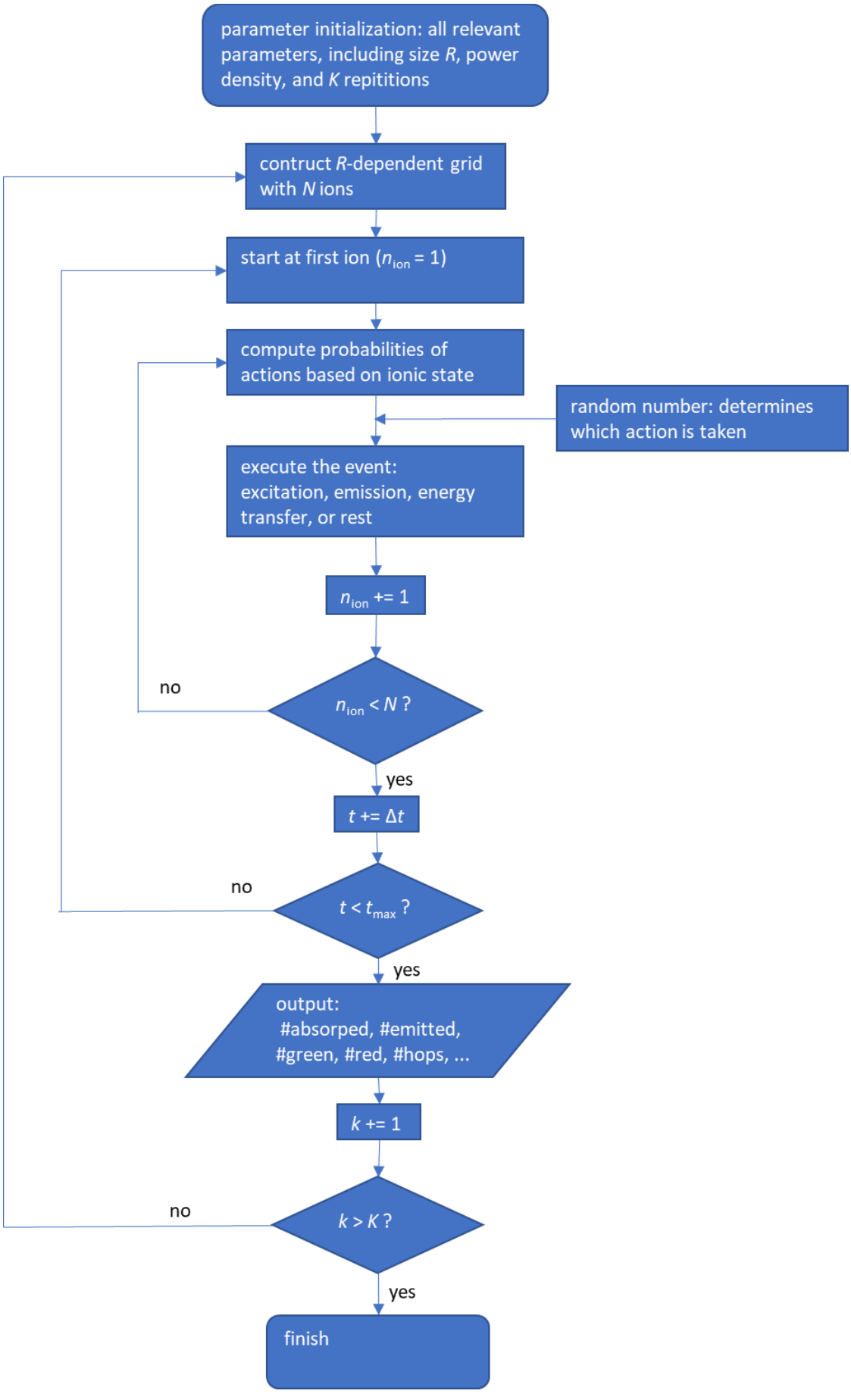

Figure S15: Flow chart of the random walk script used in this study.

Assessing the model.

With the above simplifications, we can simulate the green/red relative emission intensities of the small unshelled UCNCs (7 nm), large unshelled UCNCs (30 nm), and the bulk material, by merely adjusting the radiative rates for the emissive levels of Er^{3+} and Yb^{3+}, derived from measurements with ErNC and YbNC. The reciprocal of the measured lifetime is used as radiative rate.

Figure S16 (left panel) displays the relative emission intensities with the radiative rates of unshelled small UCNCs, larger UCNCs and bulk materials, under perfect conditions (no surface quenching, Q = 0) and using R = 15 nm. The radiative rates, obtained from time-resolved measurements, can accurately predict the P-dependent UC behavior, experimentally obtained from wavelength-resolved UCL measurements.

Next, the model is assessed regarding its potential to model surface quenching. Therefore, the quenching rate from Zuo et al.[5] is incorporated into the model and multiplied by an additional factor Q, varying between 0 and 1, to tune the degree of surface quenching, for example for thin shells, incomplete shells, or core-shell systems with lattice defects at the boundary surface. When increasing the quenching to 100 % (Q = 1), the red (i.e. three-photonic) emission almost vanishes (Fig. S16 right) with increasing quenching efficiency, three-photonic processes become more and more unlikely. Please note that our model only considers one type of quenching, where the excitation energy is deleted. Other mechanisms of UCL quenching exist, as discussed in the MS (section: ***Luminescence decay dynamics of differently sized core and core/shell YbNC and ErNC compared to single doped bulk materials***) but they are not included in this model.

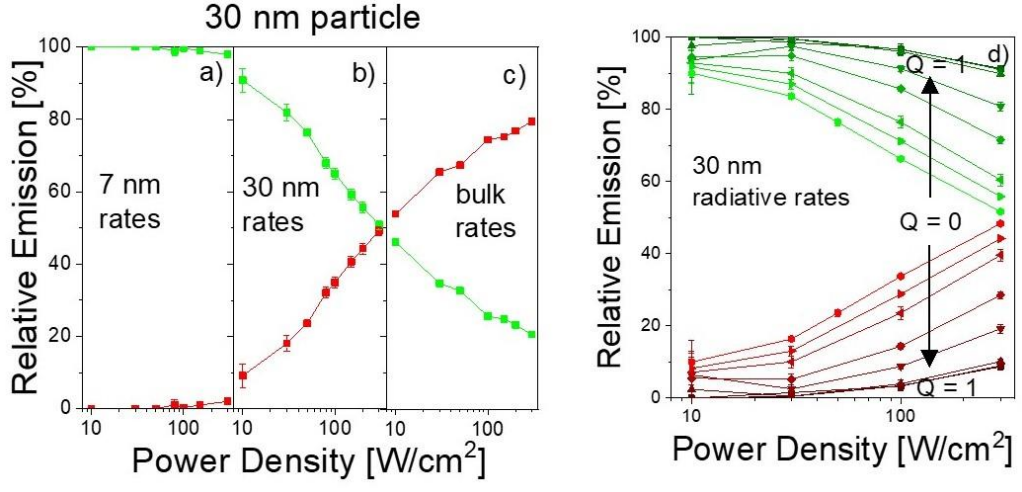

Figure S16 Relative emission intensities of two-photonic (green) and three-photonic (red) emissions of the simulated particles. Left: Relative emission intensities of an UCNC with radiative rates of (a) 7 nm UCNCs, (b) 30 nm UCNCs, and (c) bulk microcrystals, obtained with our random walk model. (d) Relative emission intensities with radiative rates of 30 nm UCNC for variation of the surface quenching rate from Q = 0 (no quenching) to Q = 1 (100 % of Zuo et al.[5]'s quenching rate), obtained with our random walk model.

Next, we investigated the mean excitation pathlength inside the particle. For every energy transfer between nearest neighbors, an interionic distance of 0.69 nm is assumed, corresponding to the average distance between the dopant ions[6]. Naturally, the mean excitation pathlength is different for different degrees of surface quenching, but it also depends on excitation power density and, as turns out here, on particle size. As a representative example, we used the 30 nm particle with its respective radiative rates, varied the quenching factor Q from 0 to 1 in various steps, and determined the corresponding average pathlength of the excitation depicted in Fig. S17.

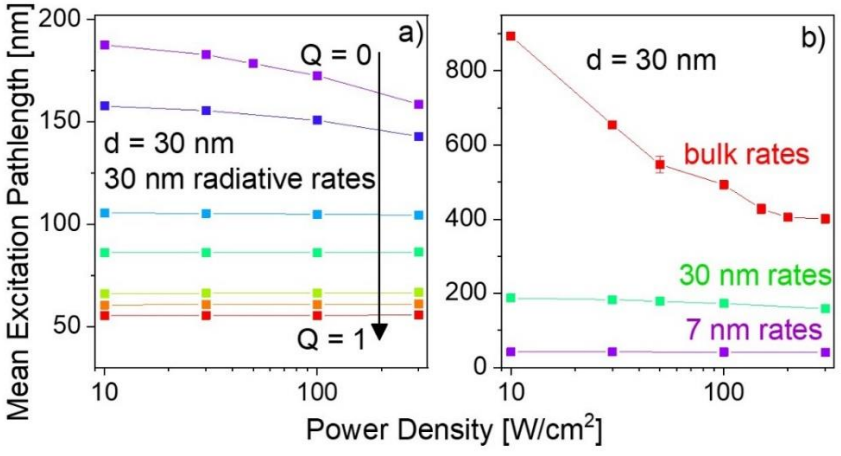

Figure S17 Mean excitation pathlengths of excitation inside the simulated particles. (a) Mean excitation pathlengths for 30 nm UCNCs with quenching rates varying from Q = 0 (no quenching) to Q = 1 (100 % of the quenching rate of Zuo et al.[5]), obtained with our random walk model with radiative rates of 30 nm UCNC. (b) Mean excitation pathlengths for 30 nm UCNCs, obtained with our random walk model using radiative rates of 7 nm UCNCs (purple), 30 nm UCNCs (green), and bulk powder (red).

The unquenched system experiences a strong dependence on excitation power density (190 nm at 10 W/cm^2, 160 nm at 300 W/cm^2 (Figure S17a)), while the fully quenched system yields an average pathlength of 55 nm for excitation power densities of 10 W/cm^2 to 300 W/cm^2. This value is in the same range as the particle size of 30 nm. Since the energy does not move in a specific direction, but can travel randomly like in a diffusion process, it is straightforward to conclude that once a quenching center at the surface is reached, the excitation is immediately quenched, and processes like emission are suppressed. While the fully-quenched system is *P*-independent due to the dominant quenching process, the unquenched system shows a *P* dependence, with shorter mean pathlengths for higher *P*, most likely due to the higher probability of multiphotonic excitation of an Er^{3+} ion when there is generally a higher number of excited ions present in the particle lattice. Extrapolating from Fig. S17(a), a drastic decrease of the mean excitation pathlength can be expected for very higher *P*. This explains why surface quenching does not play a significant role in e.g. single-particle measurements using confocal microscopes done at very high *P*.

The almost 5 x higher mean excitation pathlengths resulting for bulk radiative rates (Fig. S17b) illustrates why the bulk material is so efficient, especially at low *P*[7], because if the excitation can travel very far, it is likely that it can eventually reach an Er^{3+} ion in a higher excited state.

In our simulated 30 nm particle, the excitation can travel through the entire particle – several times even, if the surface passivation is good enough to prevent surface quenching; as a consequence, the number of excited states present at the same time, within one particle, determines how likely two- and three-photonic processes are. This is illustrated in Fig. S18, where three different sets of experimentally obtained radiative rates ("7 nm core unshelled UCNC", "30 nm core unshelled UCNC", UC-Bulk) are used to simulate the excitation dynamics in UCNC of five different sizes. For each set of radiative rates, there is a significant difference with respect to particle size. The same is true for the resulting relative emission curves depicted in Fig. S19.

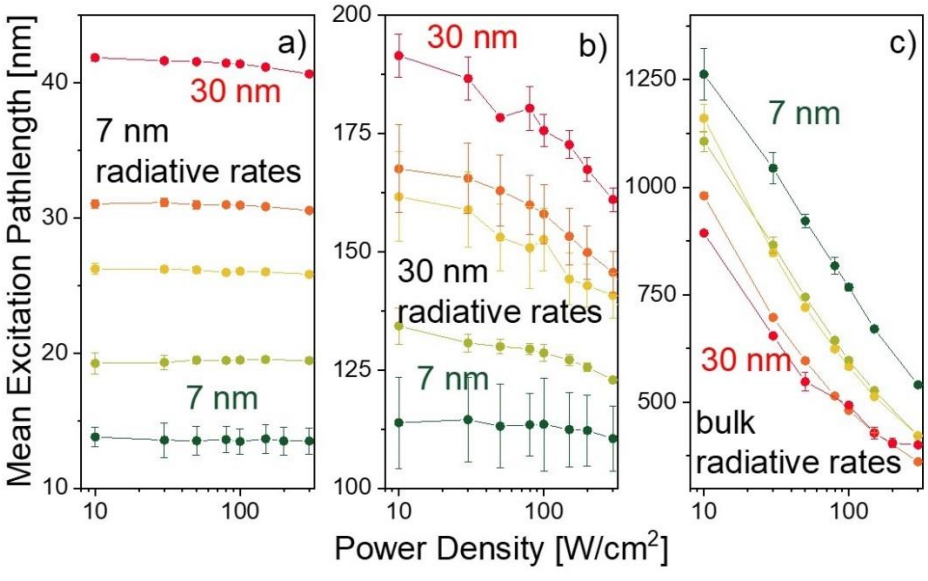

Figure S18 Mean Excitation Pathlengths for differently sized UCNC with radiative rates obtained experimentally from (a) 7 nm UCNCs, (b) 30 nm UCNCs, and (c) bulk phosphor, calculated with our random walk model with the surface quenching rate set to zero.

We observe a rather constant mean excitation pathlength with respect to *P* for the simulation with the 7 nm radiative rates (Fig. S18(a)), and a decrease of the mean excitation pathlength for increasing *P* that becomes more pronounced with increasing size for the simulation with 30 nm radiative rates (Fig. S18(b)). As mentioned above, the reason for this drop is possibly the higher probability of encounters with already-excited Er^{3+} ions for a higher number of excited ions in the host lattice, which is the case for higher *P*. In Fig. S18(c), we observe a drastic decrease in the mean excitation pathlength for increasing particle size, together with a reduction for high *P*, when bulk radiative rates are employed. These rates are very small, corresponding to very long lifetimes, yielding rather long-lived excited states. For the 7 nm particle, where the overall ion number is drastically smaller than in the 30 nm particle, there are (in total) fewer Er^{3+} ions available that are not already excited or in the highest excited state, and the excitation energy needs to travel farther to reach a suitable ion.

In contrast, larger particles show a decrease of the mean pathlength of the excitation, probably because they exhibit a higher number of Er^{3+} ions and therefore the chances for the free excitation energy to perform ET to an available Er^{3+} ion are higher than in the smaller particles.

Even though there is no surface quenching implemented within the model for $Q = 0$, the smaller particles reveal a higher green-to-red ratio than the larger ones, independent of the set of radiative rates chosen for the simulation. For all calculations that contributed to the panels of Fig. S19, the same set of parameters was used, except for the particle size, which determines the total number of ions. Thereby, it becomes evident that beside surface quenching, there is a second size-related quenching effect, namely a volume effect.

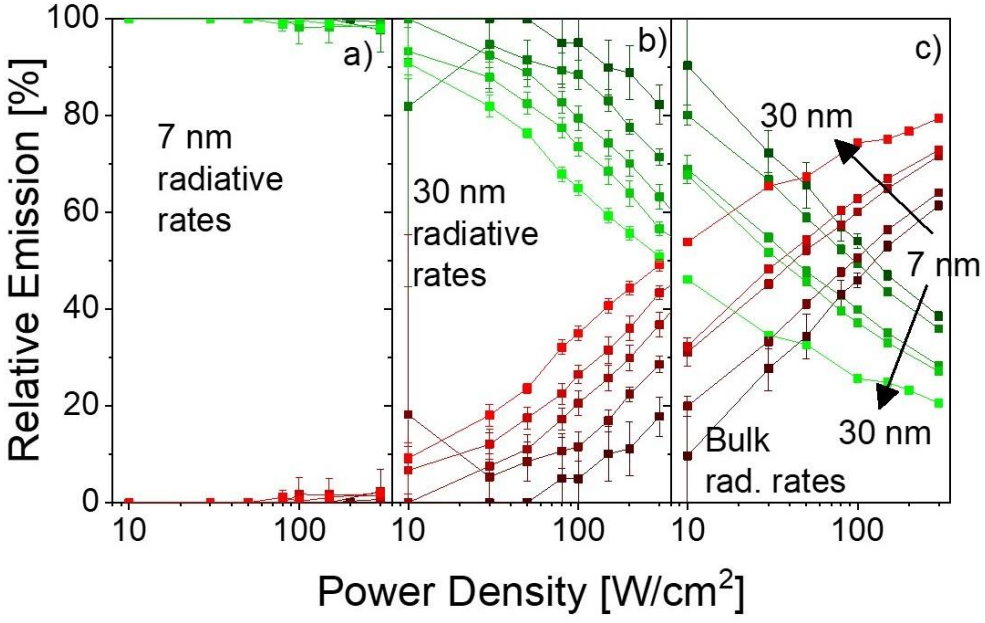

Figure S19 Relative emission intensities with radiative rates of (a) 7 nm UCNC,(b) 30 nm UCNC, and (c) Bulk microcrystalline powder, under variation of the particle size in the simulation from 7 nm to 30 nm, with the surface quenching rate set to zero, obtained with our random walk model. For all calculations that contributed to the panels of Fig. S19, the same set of parameters was used, except for the particle size, which determines the size of the nanocrystal and therefore, the total number of ions. Thereby, it becomes evident that beside surface quenching, there is a second size-related quenching effect, namely a volume effect.

References

1. Park, J., et al., *Ultra-large-scale syntheses of monodisperse nanocrystals.* Nature Materials, 2004. **3**(12): p. 891-895.
2. Rinkel, T., et al., *Synthesis of 10nm-NaYF4:Yb,Er/NaYF4 Core/Shell Upconversion Nanocrystals with 5nm Particle Cores.* Angewandte Chemie-International Edition, 2016. **55**(3): p. 1164-1167.
3. Rinkel, T., et al., *Ostwald-ripening and particle size focussing of sub-10 nm NaYF4 upconversion nanocrystals.* Nanoscale, 2014. **6**(23): p. 14523-14530.
4. Mackenzie, L.E., et al., *The theoretical molecular weight of $NaYF_4$:RE upconversion nanoparticles.* Scientific Reports, 2018. **8**.
5. Zuo, J., et al., *Precisely Tailoring Upconversion Dynamics via Energy Migration in Core-Shell Nanostructures.* Angewandte Chemie-International Edition, 2018. **57**: p. 3054-3058.
6. Fischer, S., et al., *Relation between Excitation Power Density and Er^{3+} Doping Yielding the Highest Absolute Upconversion Quantum Yield.* J. Phys. Chem. C, 2014. **118**: p. 30106-30114.
7. Kaiser, M., et al., *Power-dependent upconversion quantum yield of NaYF4:Yb3+,Er3+ nano- and micrometer-sized particles - Measurements and simulations.* Nanoscale, 2017. **9** p. 10051 - 10058.